Available online at www.sciencedirect.com
SCIENCE DIRECT®
Bioorganic & Medicinal Chemistry 13 (2005) 5171–5180
Bioorganic & Medicinal Chemistry

Synthetic multifunctional pores that open and close in response to chemical stimulation

Virginie Gorteau,[a] Guillaume Bollot,[a] Jiri Mareda,[a] Dario Pasini,[a,†] Duy-Hien Tran,[a] Adina N. Lazar,[b] Anthony W. Coleman,[b] Naomi Sakai[a] and Stefan Matile[a,*]

[a]*Department of Organic Chemistry, University of Geneva, Geneva, Switzerland*
[b]*Institut de Biologie et Chimie des Protéines, CNRS UMR 5086, 7 passage du Vercors, F69367 Lyon, France*

Accepted 6 May 2005
Available online 13 June 2005

Dedicated to Professor Koji Nakanishi on the occasion of his 80th birthday.

Abstract—Studies on synthetic multifunctional pores with external and internal active sites for ligand gating and noncompetitive blockage are presented, with emphasis on the contribution of external ligands to the characteristics of the pore. A comparison between different synthetic multifunctional pores reveals that the location of functional groups in rigid-rod β-barrel pores is precisely reflected in the function: molecular recognition at the outer barrel surface results in pore opening, while molecular recognition at the inner barrel surface results in pore closing. Negligible nonspecific leakage, disappearance of pH gating, inhibition of intervesicular pore transfer, and maybe also the flickering of currents of single open pores characterize external ligands as adhesive cushions that liberate the pore from lateral pressure exerted by the surrounding membrane. Refined molecular models show good agreement with pore design and experimental facts with regard to function.

1. Introduction

In nature, ion channels and pores open and close in response to chemical and other stimulations for transferring information across biomembranes. In the current research on the use of synthetic,[1–11] bioengineered,[12,13] and biological[14] ion channels and pores, blockage has been exploited extensively, whereas a more challenging ligand gating has so far remained elusive. Recently, however, we have introduced a synthetic multifunctional pore that opens rather than closes in response to chemical stimulation.[1] Different from the many cases of biological ligand gating that takes place on account of ligand-mediated changes in the pore/channel conformation, 'ligand gating' of synthetic multifunctional pores (i.e., pore 'activation' by chemical stimulation) occurred due to pore–membrane interactions. In other words, rigid-rod β-barrel **1** with internal HH dyads and external LRL triads was envisaged to be inactive as a pore because the external arginine arrays produced an overall hydrophilic outer surface (Fig. 1). If barrel **1** remained in the media rather than partitioning into lipid bilayer membranes, no pore activity could be observed. Binding of an amphiphilic oligoargininophile, such as fullerene **2**, was then expected to convert the polarity of the external barrel surface from hydrophilic to lipophilic. This change should cause the hydrophobic ligand–barrel complex **3** to partition into a bilayer, and desired pore activity in response to chemical stimulation could be observed.

Rigid-rod β-barrel **1** was synthesized following the methods that were adopted previously with other peptide sequences.[1] Ligand gating was studied at the

Abbreviations: AC, adhesive cushion; Ampso, *N*-(1,1-dimethyl-2-hydroxyethyl)-3-amino-2-hydroxypropanesulfonic acid; ANTS, 8-aminonaphthalene-1,3,6-trisulfonic acid (disodium salt); BLM, black lipid membrane; CF, 5(6)-carboxyfluorescein; CFD, CF-dextran; DPX, *p*-xylenebis(pyridinium)bromide; EC_{50}, effective concentration; EMP, external membrane pressure[30]; EYPC, egg yolk phosphatidylcholine; FRET, fluorescence resonance energy transfer; H, His, L-histidine; Hepes, *N*-(2-hydroxyethyl)piperazine-*N*′-(2-ethanesulfonic acid); IC_{50}, inhibitory concentration; ICR, internal charge repulsion[29]; L, Leu, L-leucine; LUVs, large unilamellar vesicles; Mes, 2-morpholinoethanesulfonic acid monohydrate; R, Arg, L-arginine; Tes, *N*-[tris(hydroxymethyl)methyl]-2-aminoethanesulfonic acid.

* Corresponding author. Tel.: +41 22 379 6523; fax: +41 22 379 3215; e-mail: stefan.matile@chiorg.unige.ch
† On leave from Department of Organic Chemistry, University of Pavia, Pavia, Italy.

0968-0896/$ - see front matter © 2005 Published by Elsevier Ltd.
doi:10.1016/j.bmc.2005.05.022

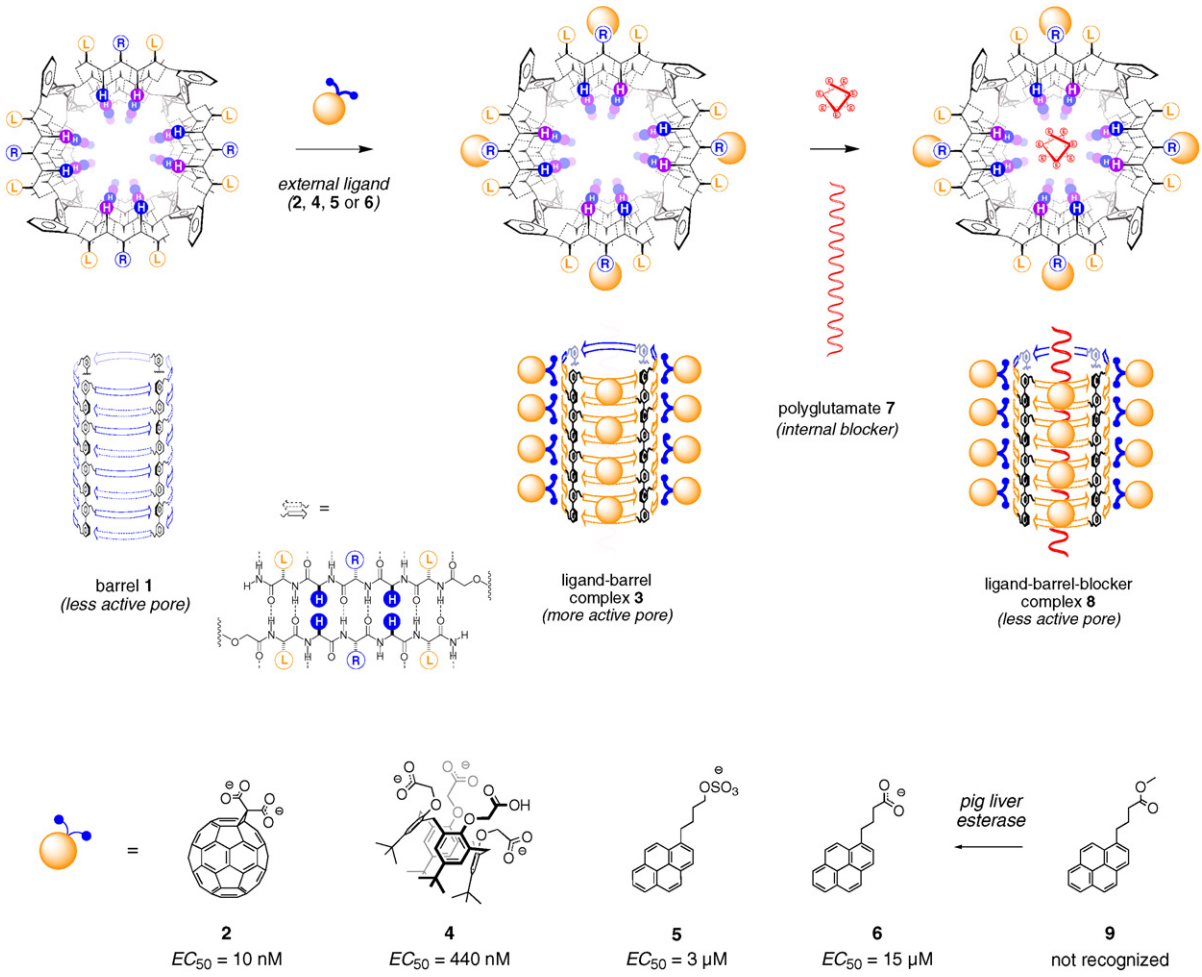

Figure 1. Activation of inactive pore **1** by external binding of amphiphilic argininophiles, such as fullerene **2**, calixarene **4**, or pyrenes **5** and **6** to maximize barrel–membrane interactions and noncompetitive blockage of active pore **3** by internal α-helix recognition of polyglutamate **7** to minimize internal space in deactivated pore **8**. Rigid-rod β-barrels are depicted in side view with β-sheets as arrows (N → C, bottom) and in axial view with β-sheets as solid (backbone) and dotted lines (hydrogen bonds, top; external amino acid residues are dark on white, internal ones white on dark, single-letter abbreviations).

functional and structural levels in EYPC LUVs, i.e., large unilamellar vesicles that were composed of egg yolk phosphatidylcholine. When added to EYPC LUVs loaded with 5(6)-carboxyfluorescein, i.e., EYPC-LUVs⊃CF, rigid-rod β-barrel **1** did not mediate any substantial efflux of self-quenched intravesicular CF. Ligand-gated formation of active pores **3** was confirmed at the functional level by an increasing CF efflux with increasing concentrations of amphiphilic oligoargininophiles, such as fullerene, calixarene, or pyrene ligands **2**, **4**, **5**, and **6**. To elucidate the structural basis of ligand gating, EYPC LUVs were labeled with acceptors of fluorescence resonance energy transfer (FRET) from intrinsic *p*-octiphenyl donors in rigid-rod β-barrel **1**. Increasing the FRET with increasing ligand concentrations confirmed the design mechanism of ligand gating, i.e., external recognition to obtain constructive pore–membrane interactions.

The internal HH dyads of pore **3**, not taking part in ligand gating, helped in noncompetitive blockage. Internal α-helix recognition by rigid-rod β-barrel **1**, exemplified by polyglutamate **7**, worked as expected and hindered the CF efflux through pore **3** (Fig. 1). A constant inhibitory concentration IC_{50} with varied effective ligand concentrations EC_{50} (Fig. 1) has demonstrated that blockage occurred noncompetitively. Constant FRET with increasing blocker concentrations was the key finding. Not only did it confirm the transformation of ligand–barrel complex **3** to ligand–barrel–blocker complex **8** as the origin of blockage, it also provided structural evidence that this process occurred in the lipid bilayer membrane. The latter observation was in agreement with previous structural studies on the blockage of synthetic multifunctional pores with DNA duplexes and pyrenetrisulfonates.[3]

The practical usefulness of such ligand gating has been demonstrated through continuous fluorometric detection of chemical reactions. Different from real-time detection, continuous detection remains problematic on account of pores acting on the blockage. Substrate **9**, however, does not interact with rigid-rod β-barrel **1** at all, and its enzymatic esterolysis into ligand **6** is detectable continuously as pore opening as a function of reaction time.

The findings summarized above have been reported in the preliminary communication on the topic.[1] The principal objective of this study was to assess the contribution of external ligands to the characteristics of rigid-rod β-barrel pores. Insignificant nonspecific leakage, suppression of intervesicular pore transfer, as well as pH insensitivity, and possibly the flickering single-pore conductances suggest that external ligands may act like adhesive cushions between the pore and membrane that absorb external membrane pressure to, e.g., prevent the pore from closing at low internal charge repulsion.

2. Results and discussion

2.1. Molecular modeling

Molecular models of the ligand–barrel complex **3** with external calixarene ligands **4** have been reported.[1] Molecular mechanics simulations with external fullerene ligands **2** produced an optimized ligand–barrel complex that was consistent with the expected structure of open pore **3** (Fig. 2). In brief, MacroModel version 7.0,[15,16] equipped with the Maestro 4.1 graphical interface,[17] was used to assemble and preoptimize (100 iterations) the barrel **1** by eliminating close contacts with the MMFF94s force field[18,19] and the Polak–Ribiere conjugate gradient (PRCG) algorithm. Geometry optimizations, along with short molecular dynamic simulations, were carried out with the AMBER 8 package[20] using *parm99* and *gaff* force fields.[21,22] Fullerene **2** and polyglutamate **7** were added to barrel **1** using the xLEaP module.[23] In each equilibration, all atoms of the complexes were free to move about. The ligand–barrel and ligand–barrel–blocker complexes obtained with xLEaP were optimized further with the Sander module (rmsd < 0.05 kcal/mol, cutoff = 50.0 Å).[20] Each complex was heated to 300 K in 10 ps using a 1.0 kcal/mol restraint and then equilibrated in a short simulation of 50 ps. The structures shown in Figures 2 and 3 were obtained after geometry optimization from an average geometry of the last 5 ps (Steepest Descent and Conjugate Gradient). Owing to the multitude of local minima on the potential energy surfaces of complexes **3** and **8**, short molecular dynamics simulations were requisite to obtain optimized structures corresponding to the lowest energy minima shown in Figures 2 and 3.

During geometry optimization, the inner diameter of pore **3** was reduced from 19.0 to 12.2 Å (Fig. 2A), a value that was in excellent agreement with the inner diameter deduced from single-pore conductances (below). The *P*-helicity of pore **3** increased slightly during optimization, and the external fullerenes adopted a regular zigzag pattern (Fig. 2C). An inspection of ligand–barrel interactions consistently revealed two hydrogen bonds from two different arginine donors of neighboring β-strands to each of the two carboxylate acceptors (Fig. 2B). In other words, one arginine donor formed two hydrogen bonds with two different fullerene ligands to provide an overall regular network that multiplies connected and presumably stabilized neighboring ligands and β-strands. Ligand–ligand interactions were dominated, as expected, by π–π interactions (Fig. 2B).

The closed pores **8** with external fullerene ligands **2** and internal α-helix blockers **7** were subjected to an identical optimization procedure (Fig. 3). To allow for internal ion pairing, histidines were protonated by 50% but polyglutamate was not protonated. During optimization, internal histidine residues shifted slightly from β-sheet staves (Fig. 2A) inward to seize the internal α-helix blocker (Fig. 3A). This side-chain motion as well as a significant barrel contraction accounted for a significant reduction in the internal diameter from 12.2 to 5.4 Å (compare Figs. 2A and 3B). External ligand–pore interactions (Fig. 2C) were not significantly affected by this internal template effect. An inspection of barrel–blocker interactions revealed hydrogen bonds from protonated and deprotonated histidine donors to carboxylate acceptors of the polyglutamate blocker. The α-helix was overall slightly bent to best fit the internal pore space available (Figs. 3A and C). Preliminary modeling with random-coil instead of α-helical polyglutamate blockers gave a drastic complex destabilization expected from a minimized functional group density in the pore.

2.2. Ligand location

To elaborate on ligand location, pore **1** with external arginines was compared with pore **10**, in which the arginines were located at the inner barrel surface. The response of rigid-rod β-barrels **1** and **10** to stimulation by calixarene **4** and other guests was totally different. Without ligand **4**, pore **1** mediated a weak CF efflux that was not effective due to passive diffusion of CF across the membrane.[1] The ability of rigid-rod β-barrel **1** to mediate the release of self-quenched CF from EYPC-LUVs⊃CF increased in the presence of increasing concentrations of calixarene **4** (Fig. 4A). Hill analysis of the dose–response curve revealed a nanomolar effective ligand concentration EC_{50} = 440 nM, as mentioned previously.[1] Rigid-rod β-barrel **10** mediated CF efflux in the absence of calixarene **4** (Fig. 4B, dotted). Pores **10** were, however, inactivated rather than activated by calixarene **4** (Fig. 4B, solid). Hill analysis gave an IC_{50} = 15 μM for calixarene **4** as a blocker of pore **10**. Ligand **4** did not promote the CF release under these conditions in the absence of pores **1** or **10** (Fig. 4).

The complementary response of these two pores to stimulation by calixarene **4** provided a wonderful illustration of how well the rational positioning of functional groups in rigid-rod β-barrel structures is functionally expressed. To rigid-rod β-barrel **1**, calixarene **4** acts as a ligand because binding to external arginine residues increases the external barrel's lipophilicity to mediate the partitioning of the barrel into the membrane to form active pore **3** (see Section 1). In rigid-rod β-barrel **10**, the external arginines of rigid-rod β-barrel **1** are replaced by external leucines, whereas every second internal histidine is replaced by internal arginines. The consequence is that pore **1** with *external* arginines is opened by, e.g., calixarene **4**, whereas barrel **10** with *internal* arginines is closed

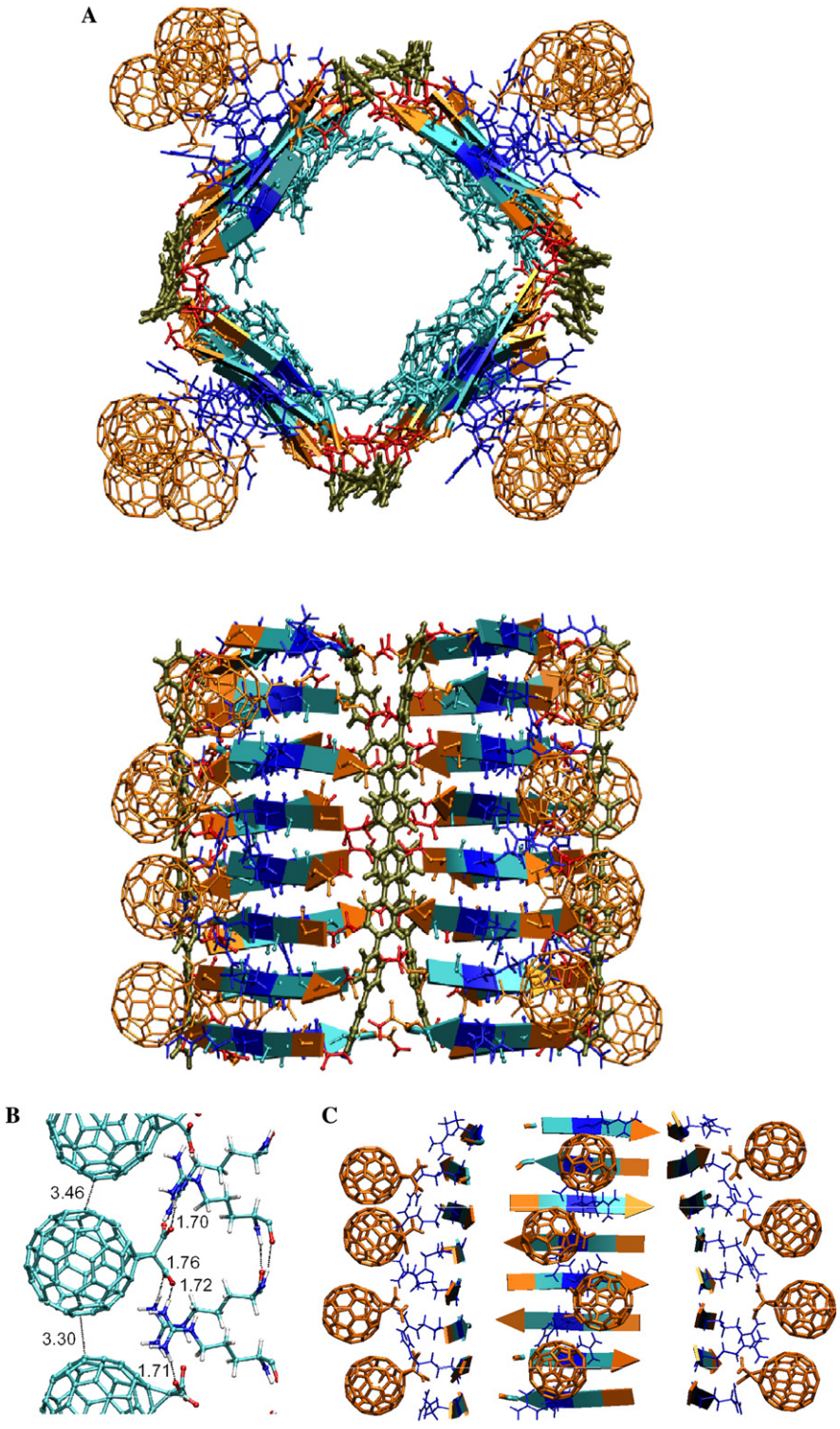

Figure 2. Optimized structure of open pores **3** with external fullerenes **2** (A) including the details of ligand–barrel and ligand–ligand interactions (B) and a simplified cutaway side view highlighting the zigzag pattern of external fullerenes (C); 100% fullerene deprotonation, 100% arginine protonation, 0% histidine protonation. (A and C) Arginines are in blue, histidines in cyan, leucines and ligands **2** in gold, β-sheets highlighted as ribbons, and *p*-octiphenyls in ball-and-stick in tan color; (B) C cyan, H gray, O red, and N blue, indicated distances given in Angstroms.

to give inclusion complex **11**. These findings corroborated that ligand recognition takes place at the outer surface of barrel **1** and contributes to, if not determines, the interactions of pore **3** with the surrounding bilayer membrane.

2.3. Effects on pore architecture

It was unlikely for the peripheral ligand location to modify the internal space of pore **3** but it could possibly disturb the bilayer to cause nonspecific leakage.

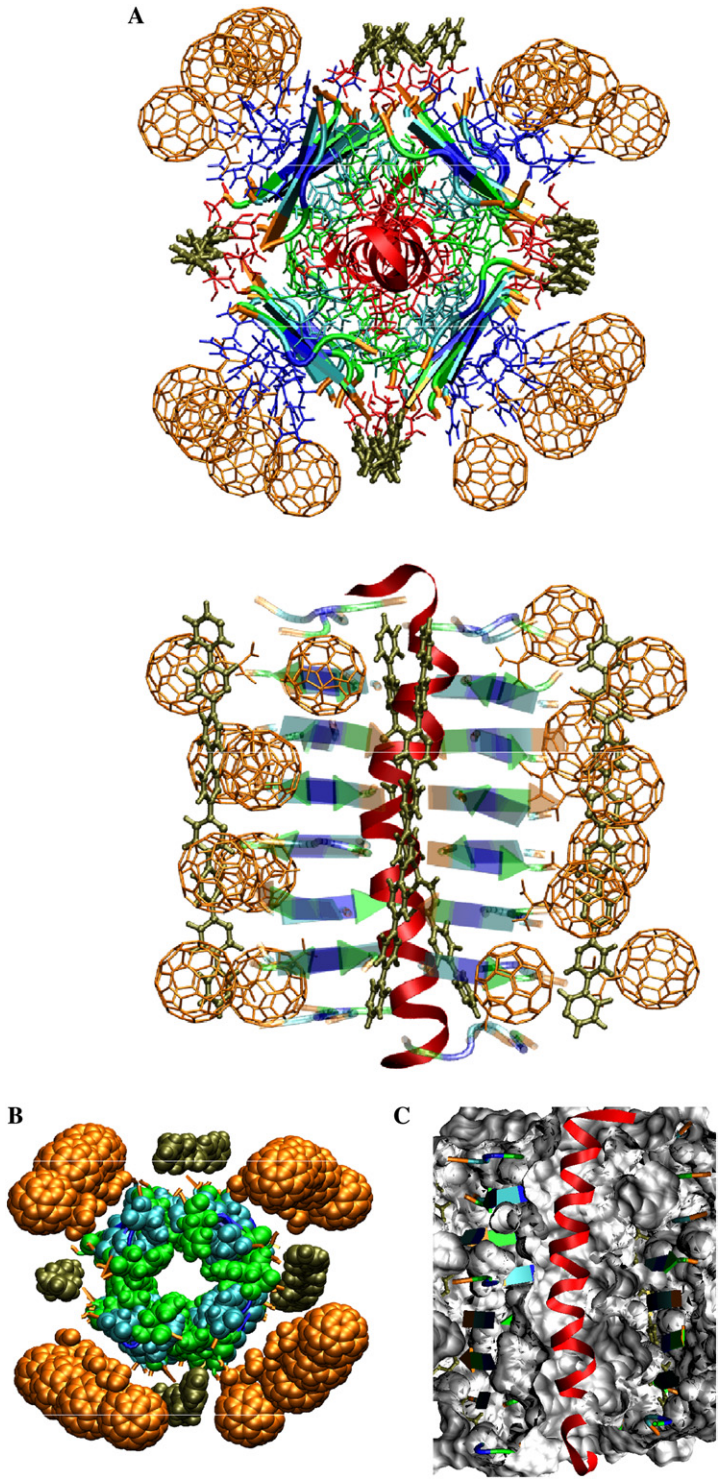

Figure 3. Optimized structure of closed pores **8** with external fullerenes **2** and internal polyglutamate helices **7** (A) including a space-filling axial view of the pore where the α-helical blocker is removed (B) and a cutaway view of the Connolly surface of the pore filled with the α-helical blocker (C); 100% fullerene deprotonation, 100% arginine protonation, 50% histidine protonation, and 0% polyglutamate protonation. Color code as in Fig. 2 with histidines in green (protonated) or cyan (deprotonated) and α-helices as red ribbons.

According to molecular models, the internal space of pore **3** is sufficient for CF to move through, whereas the translocation of molecules larger than ~1.5 nm seems to be problematic (Fig. 2). To test for either pore expansion (less likely) or membrane defects (more likely) caused by external ligands, EYPC LUVs were loaded with CF-dextran (CFD, molecular weight 13,600 g/mol), a classical probe in size exclusion experiments.[24] As for CF efflux, the CFD efflux was detected continuously by monitoring the disappearance of self-quenching upon fluorophore release into the media. The efflux of CFD mediated by pore **3** formed by calixarene **4** and barrel **1** was reduced when compared to CF efflux under nearly identical conditions (Fig. 5). Qualitative CFD

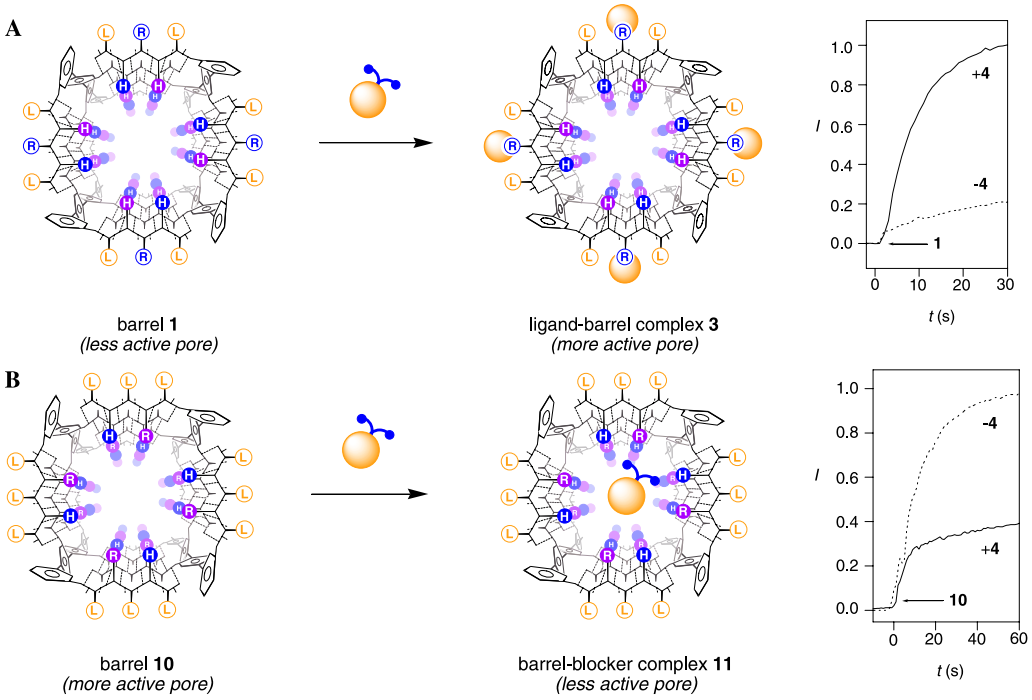

Figure 4. Functional response to the location of arginine arrays in rigid-rod β-barrel pores: external binding of argininophiles, such as calixarene **4**, to barrel **1** results in pore opening (A, EC_{50} = 440 nM);[1] internal binding of argininophiles, such as calixarene **4**, to barrel **10** results in pore closing (B, IC_{50} = 15 μM). The representative original data selected for each example show a fractional change in CF emission I (λ_{ex} 492 nm, λ_{em} 517 nm) as a function of time after the addition of barrel **1** (A, 125 nM) or **10** (B, 125 nM) and ligand **4** (dotted: 0 nM, solid: 800 nM (A), 20 μM (B)) to EYPC-LUVs⊃CF (250 μM EYPC) in buffer (10 mM Hepes, 107 mM NaCl, pH 7.0), calibrated by final lysis (excess Triton X-100).

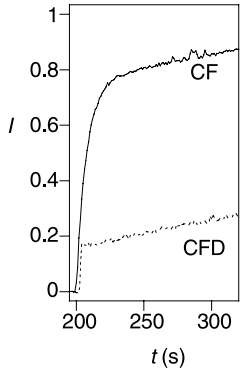

Figure 5. Size selectivity of pore **3** with external ligand **4**. The representative original data show a fractional change in emission I of CF (solid) and CF-dextran (dotted, λ_{ex} 492 nm, λ_{em} 517 nm) as a function of time after the addition of barrel **1** (125 nM tetramer) and ligand **4** (1 μM) to EYPC-LUVs⊃CF (solid) or EYPC-LUVs⊃CFD (dotted, 250 μM EYPC) in buffer (10 mM Hepes, 107 mM NaCl, pH 7.0), calibrated by final lysis (excess Triton X-100).

results with calixarene **4** were of interest because single-pore currents were available for this ligand (Fig. 6). CF/CFD size exclusion experiments were in good agreement with the magnitude of single-pore currents.

2.4. Effects on pore stability

The addition of barrel **1** alone did not change the conductance of planar EYPC membranes. Ligand **4** did not affect the conductance of planar bilayers either. The presence of single-pore currents could be observed only after the addition of both barrel **1** and ligand **4** together, that is the formation of pore **3** (Fig. 6). Compared to a short lifetime of τ = 5 ms of the single pores formed by barrel **12** without external ligands (Fig. 7),[4,25] the pores formed by complex **3** were surprisingly stable, occasionally exhibiting opening beyond 100 ms. This observation corroborated the suggestion emerging from molecular modeling (Fig. 2) that the introduction of external ligands may increase, rather than decrease, pore stability. Linear dependence of pore activity on the concentration of monomeric *p*-octiphenyls, indicative of exergonic pore formation,[26] was in agreement with this interpretation (not shown).

Different from the pores formed by other rigid-rod β-barrels with dominant and stable current levels,[2–4,26] the current of open pores **3** showed rapid and permanent flickering between many transient current levels. These single-molecule vibrations made the determination of single-pore conductance virtually impossible. The average single-pore current was calculated to a conductance of 0.25 nS that corresponded to a corrected[27] Hille[28] diameter of 7.5 Å. Clearly below the conductance of pore **12**, as well as the minimal outer diameter of CF, this value was gross underestimation. Many nonconclusive explanations for this underestimation can be perceived, including rapid conformational pore "vibrations" (below), contribution of ligands moving through the pore, contribution of subpopulations of smaller pores, and so on. In any case, maximal conduc-

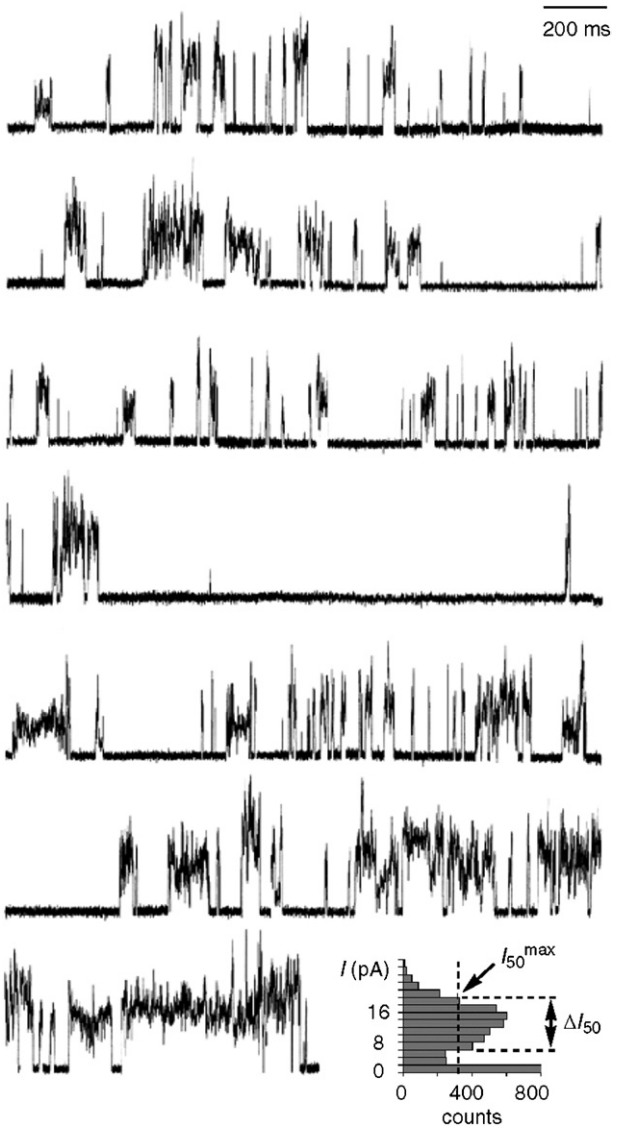

Figure 6. Planar EYPC bilayer conductance in the presence of barrel **1** (0.38 μM cis) and ligand **4** (8 μM cis, trans at ground) at +50 mV in 5 mM Tes, 1 M KCl, pH 7. Inset bottom right: single current histogram, average I = 12.5 pA, maximal I_{50} = 24 pA, ΔI_{50} = 12 pA.

tance g = 0.48 nS was calculated to a corrected inner diameter of up to 10 Å. This value was in good agreement with geometry-minimized models (Fig. 2) and CF efflux (Figs. 4 and 5).

The detectability of supramolecular architecture as complex as that of pore **3** at the single-molecule level was unexpected and quite remarkable. Interpretation of the characteristic flickering of complex **3** at the structural level was, however, not meaningful. Possible origins include transient current obstructions by ligands passing through the pore, whereas external ligand exchange could not be detected in single-molecule conductance experiments performed on internal events. Alternately, it was amusing but probably less significant to speculate that the external ligand cushions (see below) may liberate inherent vibrations of rigid-rod β-barrel pores from their suppression by external membrane pressure.

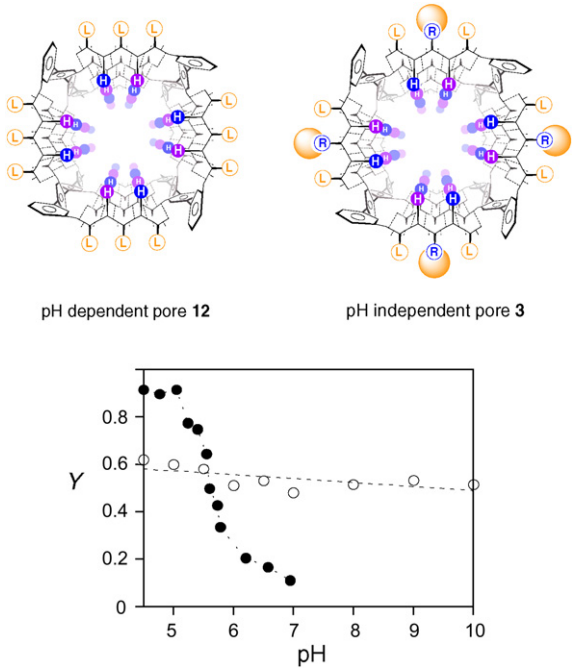

Figure 7. pH profile of ligand-gated pore **3** (63 nM tetramer, empty circles; with ligand **5**, 5 μM) in comparison to ligand-free pore **12** (filled circles, data for **12** from Ref. 29). Data at pH ⩽ 7 were obtained in 10 mM Mes buffer, data at 7 ⩽ pH ⩽ 8 in 10 mM Tes and pH ⩾ 8 in 10 mM Ampso buffers with fractional pore activity Y normalized at pH 7.

2.5. Effects on pore–bilayer interactions

The two most significant effects of external ligands on the characteristics of rigid-rod β-barrel pores relate, not surprisingly, to modified pore–membrane interactions. Suppression of intervesicular transfer—simply speaking, the jumping of barrels between vesicles—has been described previously.[1] In brief, ligand-gated pore **3**, once formed in a vesicle, does not mediate the efflux of CF from newly added vesicles. This behavior is in stark contrast to those of rigid-rod β-barrel pores with classical all-leucine surfaces, which were capable of effecting intervesicular transfer. This finding, therefore, characterized external ligands as gluey that irreversibly attache rigid-rod β-barrels to bilayer membranes.

The second key finding concerning functional consequences of external ligands was the annihilation of pH gating, a characteristic feature of classical rigid-rod β-barrel pores, such as the ligand-free pore **12** with an interior identical to that of ligand-gated pore **3** (Fig. 7). The pH profile of pore **3** was determined under the same conditions as those used for pore **12**.[29] Namely, vesicles were loaded with the pH-insensitive probes ANTS and its quencher DPX. Efflux of either the anionic ANTS or the cationic DPX is then observable in continuous fluorescence kinetics by an increase in ANTS emission as a function of time after pore addition. The ability of pore **3** to mediate ANTS/DPX efflux was pH-independent from pH 4.5 to pH 10. This pH independence contrasted sharply to the pH gating of ligand-free rigid-rod β-barrel pores in general and the

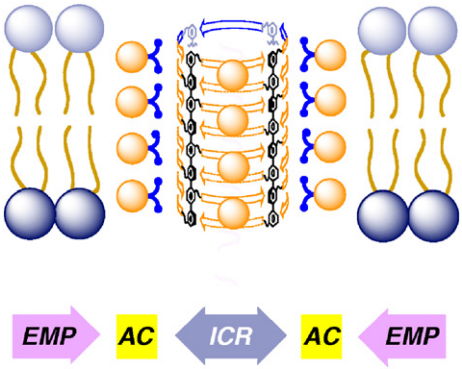

Figure 8. External ligands as adhesive cushions (ACs) in the EMP–ICR model: the limitation that intermediate internal charge repulsion (ICR) is required for maximal pore activity is overcome because ACs decouple long-range EMP–ICR interactions that cause 'implosion' of undercharged pores under lateral external membrane pressure (EMP; see Fig. 1 for pore and ligand structures).

closing of the ligand-free analog **12** at pH 5.5 in particular. Because of our interest in open rather than closed pores (and to keep the situation as simple as possible), we did not study the influence of pyrene **5** on the pH profile of pore **12**. The dependence of; IC_{50}'s on pH has been described for α-helical blockers **7** and their rigid-rid α-helix mimics.[30]

The bell-shaped pH profiles of conventional rigid-rod β-barrel pores have been rationalized in the ICR model.[29,31] It states that intermediate internal charge repulsion gives maximal pore activity, whereas insufficient and excessive ICR results in pore 'implosion' and 'explosion,' respectively. For pore **12**, for example, partial protonation of internal histidines (intrinsic $pK_a = 6.0$) is sufficient enough to open the pore.

In the context of the ICR model, the pH insensitivity of ligand-gated pore **3** came as a real surprise. The interiors of pore **3** and pore **12** are, after all, identical. However, we recently found that barrel implosion at low ICR can be triggered by lateral pressure exerted from the surrounding external membrane (EMP), whereas the same long-range EMP–ICR interactions could prevent an explosion at high ICR.[31] According to the EMP–ICR model, the pH insensitivity of ligand-gated pores **3** may, therefore, originate from a decoupling of lateral EMP by the external ligands. In other words, external ligands appear to act overall like adhesive cushions (ACs) for the enclosed pore (Fig. 8). The cushioning of lateral EMP may account for pH insensitivity, whereas gluey characteristics are demonstrated by the inhibition of intervesicular transfer. The interpretation of the fluctuating single-pore currents with the EMP-AC-ICR model is, at this stage, a pure yet amusing speculation: liberation of intrinsic dynamics of rigid-rod β-barrel pores from EMP by external cushioning.

3. Conclusion

The response of synthetic multifunctional pores **1** and **10** with external and internal active sites to chemical stimulation by guests, such as fullerene **2** or calixarene **4**, provided a persuasive illustration of how precisely the rational design of rigid-rod β-barrels is reflected in the function: molecular recognition at the outer barrel surface opens the pore, and an identical host–guest chemistry within the pore results in blockage (Fig. 4). However, the present study demonstrates that external pore design is not only a feasible approach to ligand gating, it is also of use to modulate pore characteristics without, on account of slight nonspecific leakage, causing major defects in the membrane and pore suprastructures. The most distinct impact of external ligands is in the inhibition of pH gating. Other substantial contributions include inhibition of intervesicular pore transfer and flickering in the currents of single open pores. These functional characteristics make external ligands appear like adhesive cushions between the pore and the surrounding membrane: these ligands place the pore irreversibly into the bilayer and seem to decouple the lateral external membrane pressure that contributes to the pH gating of ligand-free rigid-rod β-barrel pores. Apparently, an intriguing and admittedly unexpected third player seems to show up in the EMP–ICR model, a model under construction to rationalize and summarize the contribution of membrane–pore interactions to function (Fig. 8).

4. Experimental section

4.1. Materials and methods

Egg yolk phosphatidylcholine (EYPC) was purchased from Avanti polar lipids, ANTS and DPX were from Molecular Probes, CF, CF-dextran (MW 13,600 g/mol), 1-pyrenebutyric acid, buffers, and salts were from Sigma or Fluka–Aldrich. Reverse-phase column chromatography was performed using ODS (Fluka Silicagel 100 C18-Reverse Phase). Purity of the products was verified by using either Jasco HPLC system (PU-980, UV-970, FP-920) or Agilent 1100 Series. UV–vis spectra were measured on a Varian Cary 1 Bio spectrophotometer. Fluorescence measurements were performed either on a FluoroMax-2 or a FluoroMax-3, Jobin Yvon-Spex. The Mini-Extruder with a polycarbonate membrane, pore size 100 nm, used for LUV preparation was from Avanti polar lipids. Planar bilayer conductance experiments were performed using delrin cuvettes separated by an aperture $d = 150$ μm and connected to Ag/AgCl electrodes (Warner Instrument Corp., Hamden, CT) through agar bridges (2 M KCl) in a home-made Faraday cage. Currents were recorded with an amplifier (BC-525c) and a low-pass 8-pole Bessel filter (LPF-8) from Warner Instrument Corp., an A–D converter (DigiData 1200) and a data acquisition program (pClamp 8.0) from Axon Instruments, Union City, CA.

4.2. Synthesis of pores and ligands

Artificial β-barrels **1**[1] and **11**[32] were synthesized in 19 steps, each following the reported procedures, ligands **2** and **4** were readily prepared as described.[1] All freshly

prepared pores were purified by RP-HPLC before use. Stock solutions were prepared in MeOH or DMSO as described. The indicated pore concentration was confirmed by UV–vis spectroscopy and refers to tetramers ([pore] = [monomer]/4).

4.3. Vesicle preparation

Solutions of EYPC (25 mg) in $CHCl_3$/MeOH 1/1 (2 ml) were dried under a stream of N_2 and then under vacuum (>2 h) to form thin films. The resulting films were hydrated with 1 ml buffer A (50 mM CF, 10 mM Hepes, and 10 mM NaCl, pH 7.0, for **EYPC-LUVs⊃CF**), buffer B (7.4 mM CF-dextran, 7.4 mM Hepes, and 37 mM NaCl, pH 7.4, for **EYPC-LUVs⊃CFD**), or buffer C (12.5 mM ANTS, 45.0 mM DPX, 5 mM Tes, and 20 mM KCl, pH 7.0, for **EYPC-LUVs⊃ANTS/DPX**), for more than 30 min, and subjected to freeze–thaw cycles (5×) and extrusions (15×, Mini-Extruder with two stacked polycarbonate membranes, pore size 100 nm). Extravesicular dyes were removed by gel filtration (Sephadex G-50 for **EYPC-LUVs⊃CF** and **EYPC-LUVs⊃ANTS/DPX**, Sephacryl S300-HR for **LUVs⊃CFD**) with buffer D (10 mM Hepes, 107 mM NaCl, pH 7.0, for **EYPC-LUVs⊃CF** and **LUVs⊃CFD**, 5 mM Tes, 100 mM KCl, pH 7.0, for **EYPC-LUVs⊃ANTS/DPX**). The LUV fractions were combined and diluted to 6 ml with buffer D. Lipid concentrations were estimated from the amount of the entrapped dye. The estimated values were consistent with the earlier results of phosphate analysis. The final stock solutions had the following characteristics: ~1.3 mM EYPC; **EYPC-LUVs⊃CF**—50 mM CF, 10 mM Hepes, 10 mM NaCl, pH 7.0, inside, 10 mM Hepes, 107 mM NaCl, pH 7.0, outside; **EYPC-LUVs⊃CFD**: 7.4 mM CFD, 7.4 mM Hepes, 37 mM NaCl, pH 7.4, inside, 10 mM Hepes, 107 mM NaCl, pH 7.0, outside; **EYPC-LUVs⊃ANTS/DPX**—12.5 mM ANTS, 45.0 mM DPX, 5 mM Tes, 20 mM KCl, pH 7.0, inside, 5 mM Tes, 100 mM KCl, pH 7.0, outside.

4.4. Efflux assays

LUV stock solutions (100 μl, 1.3 mM lipid) were diluted with buffer D (1.90 ml; 10 mM Hepes, 107 mM NaCl, pH 7.0, for **EYPC-LUVs⊃CF** and **EYPC-LUVs⊃CFD**; 10 mM Mes, 100 mM KCl, pH 4.5–7.0, 10 mM Tes, 100 mM KCl, pH 7.0–8.0, or 10 mM Ampso, 100 mM KCl, pH 8.0–10.0, for **EYPC-LUVs⊃ANTS/DPX**) to give ≈13 μM lipid, placed in a thermostated fluorescence cuvette (25 °C), and gently stirred. Fluorescence emission intensity F_t (λ_{em} 517 nm, λ_{ex} 490 nm for CF and CFD; λ_{em} 520 nm, λ_{ex} 353 nm for ANTS) was monitored as a function of time (t) during the addition of guests **2** or **4** (20 μl from concentrated stock solutions in MeOH or DMSO, final concentrations as indicated), barrels **1** or **10** (20 μl from concentrated stock solutions in MeOH or DMSO, final concentrations as indicated) and 40 μl of 1.2% aq Triton X-100. Data were normalized to fractional emission intensity I using the equation

$$I = (F_t - F_0)/(F_\infty - F_0), \quad (1)$$

where $F_0 = F_t$ at pore or guest addition and $F_\infty = F_t$ at saturation after lysis. If appropriate, fractional pore activity Y (=I just before lysis) is normalized to $Y = 1.0$ for I at saturation. For ligand gating, effective concentrations EC_{50} and Hill coefficients were determined by plotting the fractional activity Y (=I just before lysis) as a function of ligand concentration and fitting them to the Hill equation

$$Y = Y_0 + (Y_{MAX} - Y_0)/\{1 + c_{LIGAND}/EC_{50})^n\}, \quad (2)$$

where Y_0 is Y without anion, Y_{MAX} is a value with an excess anion at saturation, c_{LIGAND} is the anion concentration in cuvette, and n is the Hill coefficient. For blockage, inhibitory concentrations IC_{50} and Hill coefficients were determined by plotting the fractional activity Y (=I just before lysis) as a function of blocker concentration and fitting them to the Hill equation

$$Y = Y_0 + (Y_{MAX} - Y_0)/\{1 + c_{BLOCKER}/IC_{50})^n\}, \quad (3)$$

where Y_0 is Y without an anion, Y_{MAX} is a value with an excess anion at saturation, $c_{BLOCKER}$ is blocker concentration in the cuvette, and n is the Hill coefficient.

4.5. Planar bilayer conductance experiments

BLMs were formed by painting a solution of EYPC in *n*-decane (42 mg/ml) on the 150 μm aperture pretreated with the same solution in the delrin cuvette filled with the buffer (10 mM Tes, 1 M KCl, pH 7). Currents were recorded at different holding potentials (trans at ground), low-pass filtered at 1 kHz, A–D-converted, and sampled at 10 kHz. Barrel **1** (0.38 μM) and ligand **4** (8 μM) were added to the cis chamber. All the conductance measurements were performed at room temperature (22 ± 1 °C), reliability of the employed system regularly assessed using alamethicin as a model channel (conductances of multilevel channels and voltage dependence were fully reproducible and consistent with the literature). Average and maximal conductances of pore **3** were multiplied by Sansom's correction factor[27] before application of Hille's equation[28]

$$1/g = (l + \pi d/4) \times (4\rho/\pi d^2) \quad (4)$$

where l is the ion channel length (34 Å) and ρ is the resistivity of the recording solution (ρ = 8.93 Ω cm), to give the calculated average and maximal pore diameters d 7.5 Å and 10.0 Å, respectively.

Acknowledgments

We thank A. Som, D. Ronan, and F. Perret for contributions to pore and ligand synthesis, and the Swiss NSF (including the National Research Program 'Supramolecular Functional Materials,' 4047-057496, S.M.), Delta Proteomics (A.N.L.), and the CNRS (A.W.C.) for financial support.

References and notes

1. Gorteau, V.; Perret, F.; Bollot, G.; Mareda, J.; Lazar, A. N.; Coleman, A. W.; Tran, D.-H.; Sakai, N.; Matile, S. *J. Am. Chem. Soc* **2004**, *126*, 13592–13593.
2. Sakai, N.; Mareda, J.; Matile, S. *Acc. Chem. Res.* **2005**, *38*, 79–87.

3. Matile, S.; Som, A.; Sordé, N. *Tetrahedron* **2004**, *60*, 6405–6435.
4. Sakai, N.; Matile, S. *Chem. Commun.* **2003**, 2514–2523.
5. Hector, R. S.; Gin, M. S. *Supramol. Chem.* **2005**, *17*, 129–134.
6. Mitchell, K. D. D.; Fyles, T. M. In *Encyclopedia of Supramolecular Chemistry*; Atwood, J. L., Steed, J. W., Eds.; Marcel Dekker: New York, 2004, pp 742–746.
7. Koert, U., Ed.; *Synthetic Ion Channels*. *Bioorg. Med. Chem*. **2004**; *12*, 1277–1350.
8. Boon, J. M.; Smith, B. D. *Curr. Opin. Chem. Biol.* **2002**, *6*, 749–756.
9. Gokel, G. W.; Mukhopadhyay, A. *Chem. Soc. Rev.* **2001**, *30*, 274–286.
10. Kirkovits, G. J.; Hall, C. D. *Adv. Supramol. Chem.* **2000**, *7*, 1–47.
11. Scrimin, P.; Tecilla, P. *Curr. Opin. Chem. Biol.* **1999**, *3*, 730–735.
12. Bayley, H.; Cremer, P. S. *Nature* **2001**, *413*, 226–230.
13. Terrettaz, S.; Ulrich, W.-P.; Guerrini, R.; Verdini, A.; Vogel, H. *Angew. Chem. Int. Ed.* **2001**, *40*, 1740–1743.
14. Deamer, D. W.; Branton, D. *Acc. Chem. Res.* **2002**, *35*, 817–825.
15. MacroModel 7.0, Schrödinger, Inc., Portland OR, 1999.
16. Mohamadi, F.; Richards, N. G. J.; Guida, W. C.; Liskamp, R.; Lipton, M.; Caufield, C.; Chang, G.; Hendrickson, T.; Still, W. C. *J. Comp. Chem.* **1990**, *11*, 440–467.
17. Maestro 4.1, Schrödinger Inc., Portland, OR, 2001.
18. Halgren, T. A. *J. Comp. Chem.* **1996**, *17*, 490–641.
19. Halgren, T. A. *J. Comp. Chem* **1999**, *20*, 720–748.
20. Case, D. A.; Darden, T. A.; Cheatham, III, T. E.; Simmerling, C. L.; Wang, J.; Duke, R. E.; Luo, R.; Merz, K. M.; Wang, B.; Pearlman, D. A.; Crowley, M.; Brozell, S.; Tsui, V.; Gohlke, H.; Mongan, J.; Hornak, V.; Cui, G.; Beroza, P.; Schafmeister, C.; Caldwell, J. W.; Ross, W. S.; Kollman, P. A. *AMBER 8*, University of California, San Francisco, 2004.
21. Wang, J.; Cieplak, P.; Kollman, P. A. *J. Comput. Chem.* **2000**, *21*, 1049–1074.
22. Duan, Y.; Wu, C.; Chowdhury, S.; Lee, M. C.; Xiong, G.; Zhang, W.; Yang, R.; Cieplak, P.; Luo, R.; Lee, T.; Caldwell, J.; Wang, J.; Kollman, P. *J. Comput. Chem.* **2003**, *24*, 1999–2012.
23. Schafmeister, C. E. A. F.; Ross, W. S.; Romanovski, V. *LeaP*, University of California, San Francisco, 1995.
24. Rex, S. *Biophys. Chem.* **1996**, *58*, 75–85.
25. Baumeister, B.; Sakai, N.; Matile, S. *Org. Lett.* **2001**, *3*, 4229–4232.
26. Litvinchuk, S.; Bollot, G.; Mareda, J.; Som, A.; Ronan, D.; Shah, M. R.; Perrottet, P.; Sakai, N.; Matile, S. *J. Am. Chem. Soc.* **2004**, *126*, 10067–10075.
27. Smart, O. S.; Breed, J.; Smith, G. R.; Sansom, M. S. P. *Biophys. J.* **1997**, *72*, 1109–1126.
28. Hille, B. *Ionic Channels of Excitable Membrane*, 2nd ed.; Sinauer Associate: Sunderland, MA, 1992.
29. Baumeister, B.; Som, A.; Das, G.; Sakai, N.; Vilbois, F.; Gerard, D.; Shahi, S. P.; Matile, S. *Helv. Chim. Acta* **2002**, *85*, 2740–2753.
30. Litvinchuk, S.; Matile, S. *Supramol. Chem.* **2005**, *17*, 135–139.
31. Som, A.; Matile, S., *Chem. Biodiv*. in press.
32. Sordé, N.; Matile, S. *J. Supramol. Chem.* **2002**, *2*, 191–199.